RESEARCH PAPER
Contrib. Sci. & Tech Eng, 2024, 1(4)
Homepage: https://cste.journals.umz.ac.ir/
DOI: 10.22080/cste.2024.28228.1005

Numerical Simulation of Seismic-Induced Sloshing in Water Tanks Considering Three Different Approaches

Ali Ebrahimi Hariri [1]*, Yaghoub Mohammadi [2], Alireza Soltani [3]

[1] *University of Mohaghegh Ardabili, Ardabil, Iran.*

[2] *School of Mechanical, Aerospace and Civil Engineering, The University of Sheffield, Sheffield, UK.*

Article Info
Received 18 December 2024
Accepted 30 December 2024
Available online 05 March 2025

Keywords:
Rectangular Tank;
Sloshing Height;
Upward Roof Force;
Energy Dissipation Ratio;
Burial Rate;
Baffles.

Abstract:
This study investigates the factors impacting the sloshing phenomenon of the tank structures, including geometry, burial rate, and installation of T-shaped baffles under two different earthquake records. The results indicate that the tanks with larger dimensions will experience less sloshing height. Moreover, length, height, and the freeboard, respectively, are effective in lowering the roof force. However, the freeboard plays a more critical role than the tank's burial rate in reducing the roof force. Note that the roof force decreases as the freeboard and burial rate increase. The results show that lowering the height-to-length ratio of the tank reduces the maximum sloshing height. Finally, using the energy dissipation ratio concept, it is observed that the tank with baffles shows much better performance with the energy dissipation ratio of about 96%, compared with the burial approach in which even the tank under 100% burial rate just dissipates less than 50% the energy induced by the sloshing waves.

***Corresponding Author:** aliebrahimihariri@uma.ac.ir

Supplementary information: Supplementary information for this article is available at https://cste.journals.umz.ac.ir/

Please cite this paper as: E. Hariri, A. , Mohammadi, Y. , & Soltani, A. (2024). Numerical simulation of seismic-induced sloshing in rectangular water tanks considering three different approaches.. Contributions of Science and Technology for Engineering, 1(4), 16-27. doi:10.22080/cste.2024.28228.1005.

1. Introduction

Liquid storage tanks are crucial structures of modern society. They store liquids as water reservoirs or supply gas and oil for industry use. When applied during seismic excitations, sloshing waves threaten the safety of these critical structures. The applied sloshing wave causes violent fluid motions and high-impact pressure that disrupt the liquid storage tanks' integrity and safe responses. Different analytical, numerical, or experimental methods are utilized to solve the fluid storage tanks' responses affected by the sloshing phenomenon.

Due to the lack of numerical methods in the early nineties, researchers solved the sloshing problem using analytical techniques such as Westergaard, Jacobsen, Hazner, etc. [1], [2]. However, these analytical solutions were associated with many difficulties due to the complex equations governing the sloshing phenomenon.

Further, the finite element method was used to develop numerical solutions for the differential equations governing the sloshing phenomenon. Based on the proposed numerical solutions, this study includes finite element methods to study geometric characteristics, burial percentage (soil-structure interaction effects), and baffle insertion effects on the sloshing waves' amplitudes in liquid storage tanks.

Investigating the tanks' geometric dimensions, Moslemi et al. conducted a nonlinear sloshing analysis of rectangular liquid storage tanks by investigating 3D geometry, tank aspect ratio, bidirectional loading, corner sloshing, and earthquake frequency content by applying FE analysis considering fluid-structure interaction. The results suggest that the nonlinearity of sloshing could substantially influence the seismic response of shallow tanks [3]. Alfanda and Farouk studied the efficiency of rectangular or circular tanks to investigate inferences about shape effectiveness, relative cost effects of various tank types, and structural capacities. The paper shows that circular-shaped tanks are preferable to rectangular ones, but other factors must be regarded [4]. Kim et al. developed analytic solution methods to examine the dynamic response of partially filled rectangular tanks under seismic loads. Considering the flexibility and length-to-height ratio of the walls, the variation of dynamic response characteristics was investigated [5]. Chern et al. developed a pseudospectral σ-transformation model to comprehensively study the sloshing waves in a 3D rectangular tank by considering factors including base aspect ratio, excitation frequency, etc.

*ISSN **3060-6578***

The results demonstrated that the base aspect ratio played a crucial role in sloshing heights in shallow water tanks, contrary to the deeper ones. Moreover, wave regimes were observed when small amplitude resonant excitation was imposed on a shallow water tank with a non-square base [6]. Camnasio et al. conducted an experimental study on velocity fields of rectangular shallow tanks by testing a broad range of length-to-width and expansion ratios. Depending on the combination of both ratios, five various forms of flow patterns were detected [7]. Ghateh et al. offered a systematic approach to determine the seismic response factors for elevated water tank sizes and RC pedestal dimensions. Conducting Push-over analysis on 48 prototypes selected according to the codes and standards, the effect of height-to-diameter ratio, tank size, and other factors were investigated. The result indicated that the tank size had a tremendous impact on the seismic response, and two separate cracking patterns based on the height-to-diamete ratio of the pedestal were detected [8]. Hadj-Djelloul and Djermane studied the impact of local geometric imperfection on dynamic buckling in elevated water tanks. Performing 3D finite element analysis of the perfect and imperfect tanks to estimate the critical PGA, various instability criteria were considered, including the local geometric imperfection, the material and geometric nonlinearity, and nonlinear time history analysis. The numerical results show that the estimated critical PGA for the imperfect elevated water tank is 45.45% less than without the local geometric imperfection [9].

In addition to the geometric characteristics, the effects of reservoir burial rate and soil-structure interaction have also been the subject of various studies. The results demonstrated that full tanks had lower displacements than empty ones, and the pattern of soil cracks was detected [8]. Cheng et al. carried out an analysis regarding the seismic reliability of over-ground and buried concrete rectangular liquid storage structures (CRLSSs), considering the wall thickness and internal liquid depth as random variables and employing the Monte Carlo FE method. The study indicated that with the increase of wall thickness and liquid depth, the seismic reliability increases and decreases, respectively [9]. X. Cheng et al. investigated a buried horizontal double-layer SF-type liquid storage tank's dynamic response by considering liquid-solid interaction in the FEM analysis of the 3D model of the tank. The paper reveals that the seismic behaviors of the inner layer, interlayer, and outer layer are not the same under a similar earthquake [10]. Yu et al. suggested an analytical solution to obtain the dynamic response of an underground rectangular fluid tank with an elastic foundation under arbitrary dynamic loads. Applying the solution, the tank's deflection, bending moment, and shear force were evaluated [11].

In addition to modifying the geometric and burial characteristics, researchers also tried to reduce the amplitude of the sloshing waves by installing baffles as dampers. Wang et al. investigated a novel Tuned Liquid Column Damper-Inerter (TLCDI) for an SDOF system. The parametric optimization results demonstrate average decreases in acceleration responses and peak displacement compared to the TLCDs [10]. Conducting numerical and experimental examination of tuned liquid damper (TLD) to restrict the vibration of the elastic supporting structural platform (SSP) by varying the mass and frequency ratio of TLD to the SSP, Dou et al. showed that the roof plate peak displacement of considerably decreased, and a frequency shift was observed due to the TLD installed on the SSP [11]. In a paper, Jin et al. conducted an experimental investigation to study the viscosity effect on the sloshing response of a rectangular tank partially filled with water and glycerin under resonant and off-resonant excitations at different temperatures. It was observed that for a specific viscosity threshold, the sloshing slowly changes from the resonant-steady state to the harmonic [12]. In another related research, Shekari investigated the resonant sloshing responses in the baffled steel cylindrical tanks, partially liquid-filled, shaken by long-period ground motions. [13]. Yu et al. studied the effectiveness of baffles in controlling parametric sloshing and the damping of baffles under low- and high-frequency excitations. They showed that as the position of the baffles is closer to the nodes of sloshing modes, the damping effect is more noticeable [14]. Using a T-shaped baffle in a two-dimensional rectangular tank, Ünal et al. conducted a numerical study to compare the sloshing response with the case in which no baffle has been implemented. The results showed that if the tank's height is 80% of the liquid level, the baffle will decrease the pressure and dampen the liquid's wave [15]. Aghajanzadeh et al. consider the sloshing height and hydrodynamic pressure in roofless and roofed liquid storage tanks utilizing a coupled FE-SPH technique [16].

The current study applied three different approaches to control sloshing height for the first time, including geometry, burial, and baffle approaches. The results of each of them were compared using the concept of energy dissipation ratio. Specifically, first, the effect of geometry and dimensions on the tank's response to earthquakes, including sloshing height, is investigated. Next, based on the geometry section, for a tank with specific dimensions under earthquake, two approaches of burial and implementation of T-shaped baffles are considered, and the sloshing height is examined. Finally, using the energy dissipation ratio, the efficiency of each of the three methods in controlling sloshing height is studied.

2. Numerical Methods

This study employs the Lagrangian method to formulate both the fluid and structure domains.

2.1. Fluid Formulation

The Lagrangian fluid is assumed to be linearly elastic, inviscid, and irrotational. The general two-dimensional stress-strain equation of a fluid element is [20]:

$$\begin{Bmatrix} P \\ P_Z \end{Bmatrix} = \begin{bmatrix} C_{11} & 0 \\ 0 & C_{22} \end{bmatrix} \begin{Bmatrix} \varepsilon_V \\ W_Z \end{Bmatrix} \quad (1)$$

P is the pressure, P_z is the rotational stress, C_{11} is the bulk modulus of fluid, C_{22} is the constraint parameter related to W_z, ε_V is the volumetric strain, and W_z is the rotation about the axis Z.

Considering the pressure at the fluid-free surface due to the sloshing effects, its stiffness matrix is calculated by discretizing the following Equation.

$$P = \gamma_W U_{fn} \quad (2)$$

where γ_w is the weight density of the fluid and U_{fn} is the normal component of the free surface movement. In the following, the fluid total strain energy is employed to obtain the finite element approximation:

$$\Pi_e = \frac{1}{2} U_f^T K_f U_f \quad (3)$$

$$K_f = \sum k_f^e \quad (4)$$

$$k_f^e = \int_V B_f^{eT} C_f B_f^e dV^e \quad (5)$$

where U_f is the nodal movement vector, K_f is the stiffness matrix of the fluid system, K_f^e is the fluid element stiffness matrix, C_f is the elasticity matrix consisting of diagonal terms in Equation 1, and B_f^e is the strain-displacement matrix of the fluid element. In addition, the free surface motion intensifies the system's potential energy, which is considered as follows:

$$\Pi_S = \frac{1}{2} U_{sf}^T S_f U_{sf} \quad (6)$$

$$s_f = \sum s_f^e \quad (7)$$

$$s_f^e = \rho_f g \int_A h_s^T h_s dA^e \quad (8)$$

where U_{sf} and S_f are the vertical nodal displacement vector and the stiffness matrix of the free surface of the fluid system, respectively. S_f is the sum of the stiffness matrices of the free surface fluid elements, S_f^e is the stiffness matrix of the free surface fluid element, h_s is the vector consisting of interpolation functions of the free surface fluid element, ρ_f is the mass density of the fluid, and g are and the acceleration due to gravity. Furthermore, the kinetic energy of the system can be written as:

$$T = \frac{1}{2} \dot{U}_f^T M_f \dot{U}_f \quad (9)$$

$$M_f = \sum M_f^e \quad (10)$$

$$M_f^e = \rho_f \int_V H^T H dV^e \quad (11)$$

where $\dot{U}_f$ is the nodal velocity vector, M_f is the mass matrix of the fluid system, M_f^e is the sum of the mass matrix of the fluid elements, and H is the matrix consisting of interpolation functions of the fluid element.

Finally, the fluid finite element formulation of motion is calculated by the combination of Equations 3, 6, and 9 as follows:

$$M_f \ddot{U}_f + K_f^* U_f = R_f \quad (12)$$

where $\ddot{U}_f$, U_f, K_f^* and R_f are the nodal acceleration, the nodal displacement, the system stiffness matrix including the free surface stiffness, and the time-varying nodal force vector for the fluid system, respectively.

2.2. Fluid-Structure System

The coupled equations of the fluid-structure system are obtained considering the boundary condition at the fluid-surface interface:

$$U_n^+ = U_n^- \quad (13)$$

where U_n^- and U_n^+ are the normal portions of the interface structure and fluid displacement, respectively. By considering the interface condition and damping effects, the equations of motion of the coupled system to ground motions are written as [17]:

$$M_C \ddot{U}_C + C_C \dot{U}_C + K_C U_C = R_C \quad (14)$$

where M_c, C_c, and K_c are the mass, damping, and stiffness of the coupled system. U_C, $\dot{U}_C$, and $\ddot{U}_C$ are the vectors of the displacement, velocity, and acceleration, respectively. R_C is also forces applied to the coupled system.

3. Numerical Models

This section presents the numerical models' properties for investigating the geometric dimensions, the burial percentage, and the baffle insertion, including geometric characteristics, material properties, and seismic loads. Different freeboards and boundary conditions are assumed. All tanks and liquid nodes are tied in the Z-direction, moving in the longitudinal direction X and the vertical direction Y. The seismic excitations are only applied in the X-direction. The contact elements simulate the tank's interactions, including body water, body roof, water roof, and body soil.

3.1. Geometric Characteristics

This section introduces geometric dimensions, boundary conditions, and other related issues of the developed numerical models for the geometric effect, the burial percentage effects, and the baffle implementations.

3.1.1. Numerical Models for Geometric Effects

The effects of the geometric properties are studied, and the numerical tank models are categorized into two groups with two different liquid heights of 5m and 10m. All tanks are short as the H (height of the contained liquid) to L/2 (half of the tank length) ratio varies from 1 to 1/3. The thickness of all concrete tank walls (tw) is 0.5m. The tank height (Hw) is also determined based on the fluid height (H) and the freeboard. The roofless tanks have sufficient freeboards. Table 1 shows the dimensions of the tank models considered to investigate the effects of geometric properties.

All tanks are simulated with and without a roof. Figure 1 shows the schematic views of these two different tanks (roofless and roofed). The roofed tanks have some bounded freeboards (1.00m, 0.75m, 0.50m,0.25m, and 0.00m), and the roofless tanks' freeboard height is 2m. All the bottom nodes of the floor slab in all directions are restrained. The body and roof interfaces with the water are assumed to be frictionless, but the internal friction angle between the body and the roof is 45 degrees.

Table 1. Dimension of tank models for the geometric properties' effects

Group	Names	L (m)	H (m)	2H /L	Number of element
	H5L10	10	5	1	2482

Group 1	H5L15	15	5	2/3	3795
	H5L30	30	5	1/3	7718
Group 2	H10L20	20	10	1	9368
	H10L30	30	10	2/3	13948
	H10L60	60	10	1/3	27688

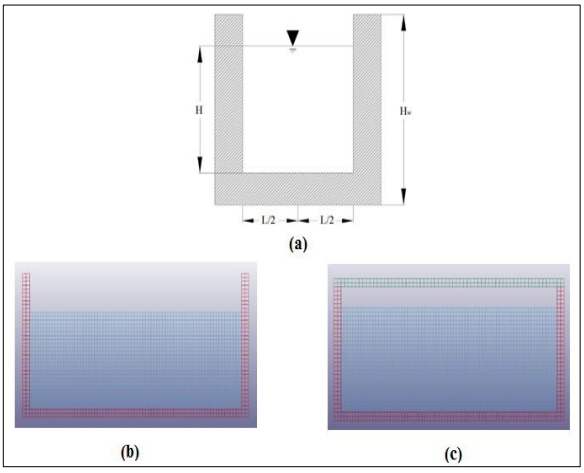

Figure 1. The schematic representation of the tank. (a) The parametric dimensions, (b) The unroofed tank, (c) The roofed Tank

3.1.2. Numerical Models for Burial Percentage Effects

Considering different burial percentages, the H5L30 model (Table 1) was selected for the burial effects investigations. The friction is ignored on the interfaces between the water and the structure, but the internal friction angle of the soil-structure interfaces is 45 degrees. Figure 2 shows the finite element simulation of the H5L30 model with its corresponding foundation. The thickness of the container walls is considered 0.5m. The soil foundation nodes are also defined as viscous boundary conditions constrained in all directions except the x-direction.

This section considers the liquid storage tank H5L30 with baffles. The selected dimensions of the baffles and their arrangement are based on the optimal dimensions presented by Ünal et al. [18] (Figure 3). Note that the tank is analyzed in case of no burial condition, assuming it is a roofed or roofless tank.

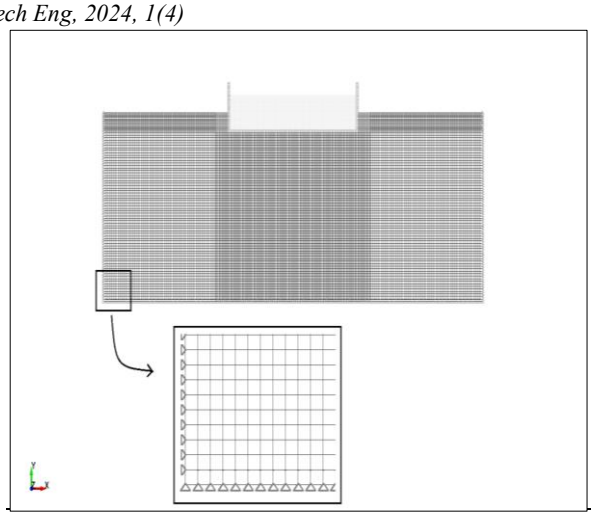

Figure 2. 2D rectangular tank model (H5L30) in the form of a two-dimensional design in perfectly buried condition, and the model of water with viscous boundaries in the software [18], [19]

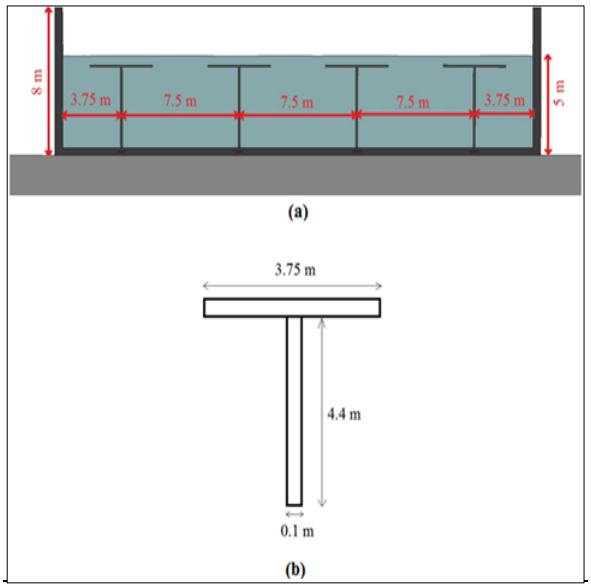

Figure 3. The schematic presentation of the baffled tank and the dimensions of the baffles

3.2. Material Properties

Table 2 presents the properties of water, concrete, and soil, which are assumed to be elastic. The contact elements are modified for all surface contacts, such as the contact surface of water and container wall, container and soil, and made ground soil and container.

Table 2. Material properties of water, concrete and soils [3, 18, 20]

Water	**Mass density (kg/m^3)**	**Viscosity coefficient (Pa)**	**c (m/s)**	**γ0**	**a**	**S_1**	**S_2**	**S_3**
	997	**0.001**	**1480**	**0.5**	**0**	**2.56**	**1.986**	**1.2268**
Concrete	Mass density (kg/m^3)	Young's modulus (Pa)	Poisson's ratio	damping				
	2300	2.66E10	0.17	5%				
Foundation Soil (S3)	Mass density (kg/m^3)	Young's modulus (Pa)	Poisson's ratio	damping	vs(m/s)	vp (m/s)		
	1900	5E8	0.35	10%	120.82	295.95		
Made ground soil	Mass density (kg/m^3)	Young's modulus (Pa)	Poisson's ratio	damping	vs(m/s)	vp (m/s)		
	1800	7.5E7	0.4	7%	309.22	643.68		

3.3. Seismic Loads

Two different recorded ground accelerations, including 1999 Kocaeli and 1994 Northridge, are applied, and Figure 4 demonstrates their time histories. In this study, PGA values for both records are scaled at 0.3g. Based on the classification proposed by Elnashai and Di Sarho [24], there are three categories which are: 1- low ratio when PGA/PGV<0.8, 2- Intermediate ratio including 0.8<PGA/PGV<1.2, and 3- High ratio including PGA/PGV>1.2. The PGA/PGV is less than 0.8 for the Kocaeli earthquake, whereas the ratio is about 0.8 for the Northridge earthquake.

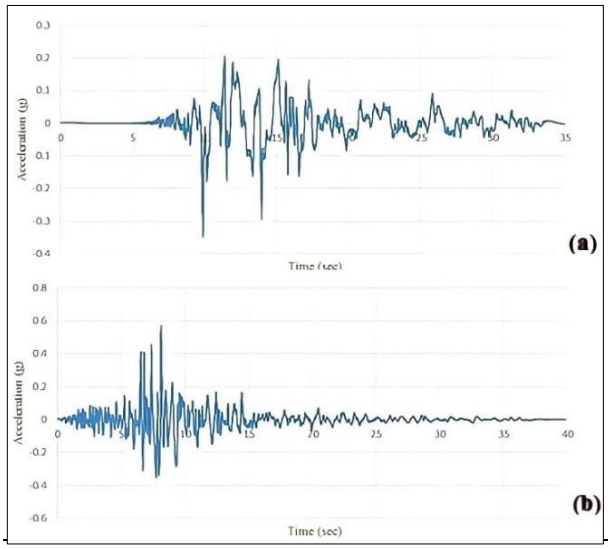

Figure 4. Two earthquake records were used in the modeling. (a) The horizontal component of the 1999 Kocaeli earthquake, (b) The horizontal component of the 1994 Northridge earthquake

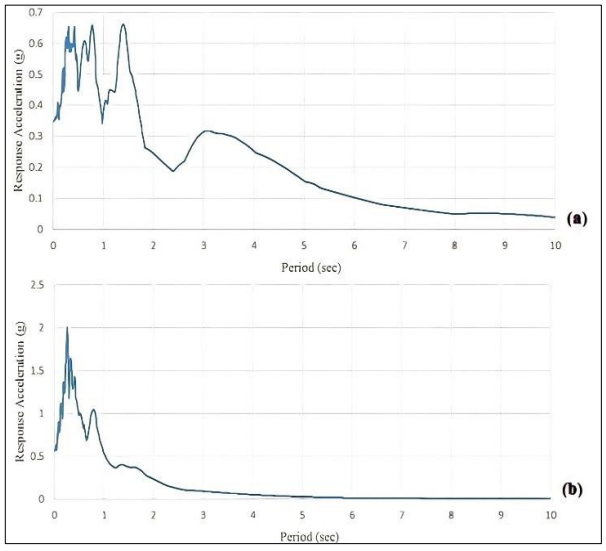

Figure 5. Two earthquake response spectrum accelerations. (a) The 1999 Kocaeli earthquake, (b) The 1994 Northridge earthquake

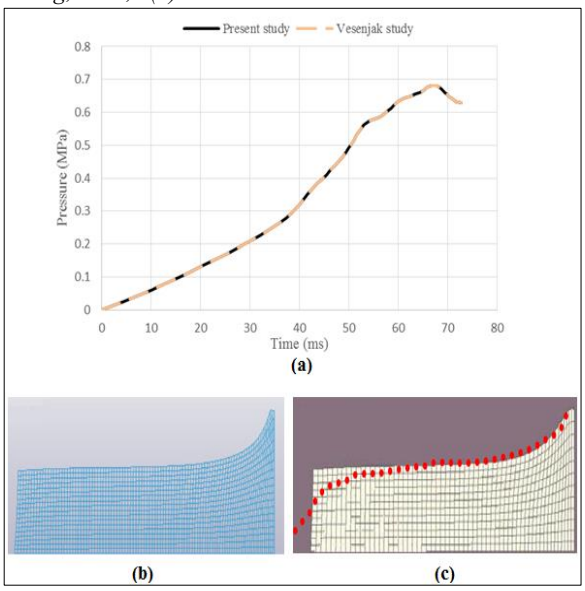

Figure 6. (a) The time variation of water pressure [21]; The free surface of the water under 30g seismic excitation at the time 30 ms: (b) the result of the made model in this study, and (c) Vesenjak article result [21]

4. Verification of Numerical Models

The results, presented by the finite element model developed in this study, are verified by the study conducted by Vesenjak et al. [21], as shown in Figure 6. Using Lagrangian, Eulerian, ALE, and SPH methods, they obtained the surface wave profiles created by stimulating a plexiglass water tank. The tank's length, width, and height were 1008mm, 196mm, and 300mm, respectively, while 60 per cent of the tank (180mm) was full of water. Then, the tank was subjected to a horizontal acceleration of 30g for 80 milliseconds, and the point with the depth of 52 mm shows the time variation of water pressure.

The current paper applies the same method used by Vesenjak et al., the Lagrangian method, comparing the obtained results in Figure 6 [21] with those calculated by the authors. The time variation of water pressure fits the Vesenjak et al. responses precisely, as shown in Figure 6-a. Also, Figure 6 presents the water-free surface under 30g seismic excitation at 30ms for both models, indicating that the developed model fits well with the results obtained by Vesenjak et al.

5. Results and Discussions

5.1. The Geometric Dimension Effects

This section focuses on the geometric dimension effects of liquid storage tanks on the responses to the sloshing phenomenon. The results include sloshing height in roofless tanks and the upward forces in roofed tanks.

5.1.1. Sloshing Height

Figure 7 shows that the maximum sloshing height decreases with increasing the tank length for the constant H. Furthermore, for the fixed L, the maximum sloshing height increases with increasing the tank height. Hence, decreasing the H-to-L ratio of the tank leads to reducing the maximum

sloshing height. For two different earthquake records, 1999 Kocaeli and 1994 Northridge, at the same scaled PGA, the Kocaeli earthquake record's sloshing height is much higher than the Northridge one. It seems the frequency content of the seismic excitation has significant effects on the sloshing phenomena.

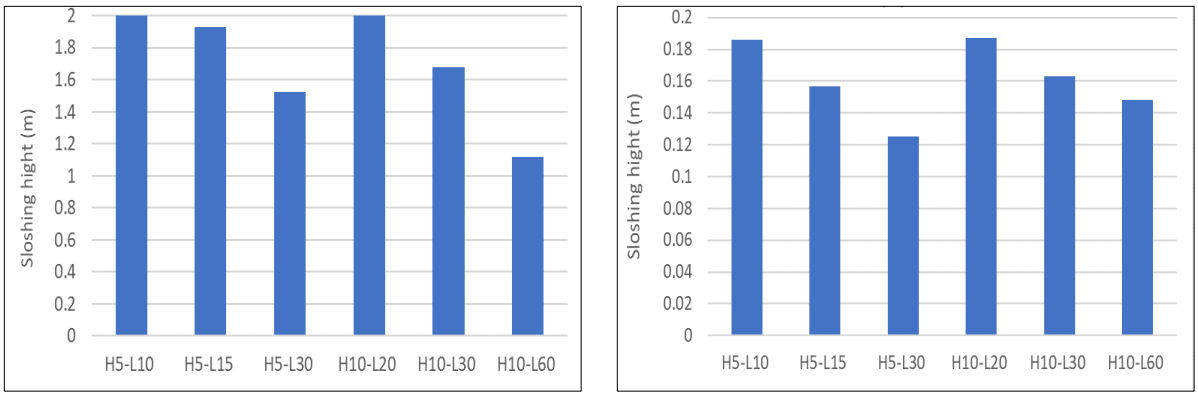

(a) (b)

Figure 7. Maximum sloshing height under a) Kocaeli 0.3g, and b) Northridge 0.3g scaled excitation

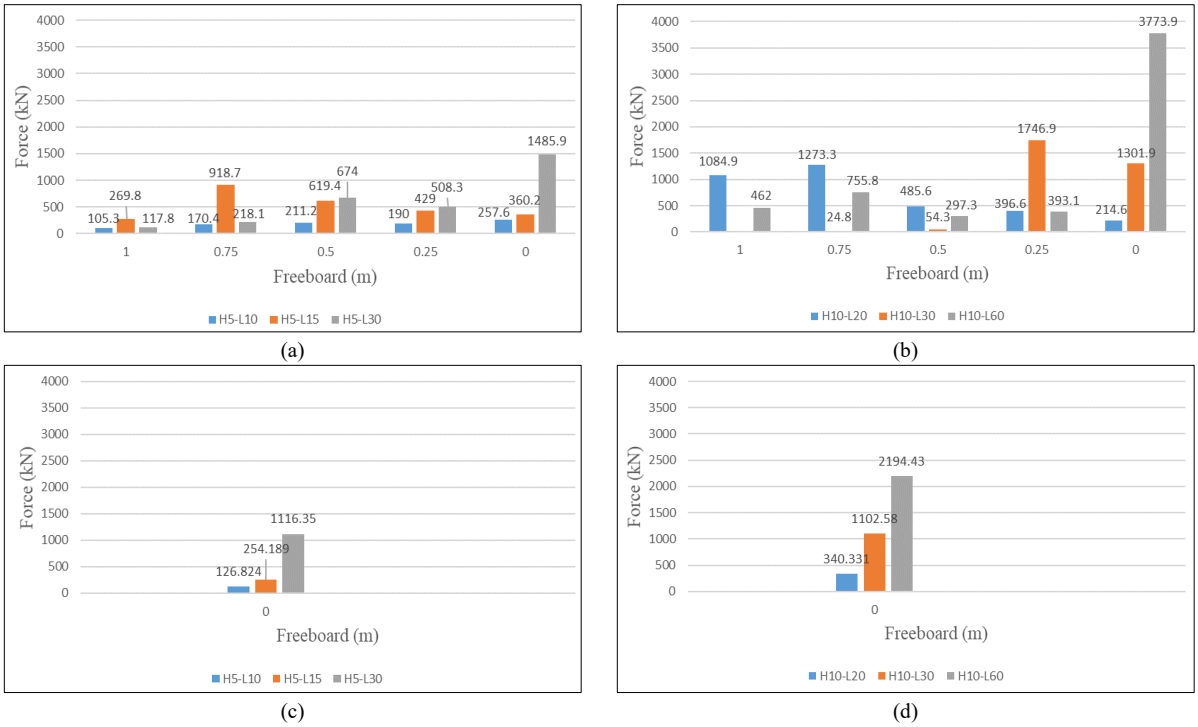

(a) (b)

(c) (d)

Figure 8. Maximum sloshing forces under 0.3g scaled ground motions for different freeboard assumptions under a) Kocaeli excitation group 1, b) Kocaeli excitation group 2, c) Northridge excitation group 1 and d) Northridge excitation group2

5.1.2. Freeboard Sufficiency and Sloshing Upward Force

This section investigates the freeboard sufficiency of roofed tanks, considering the two groups of tanks introduced in Table 1 for freeboards, varying from 0m to 1m at increments of 0.25m. The results show that both maximum sloshing height and sloshing force peak values occur on the sides of the tank wall. Figure 8 presents the upward forces in different tanks under 0.3g scaled ground motion.

The zero-force values indicate that the water inside the tank did not collide with the roof during the earthquake. A comparison of these zero sloshing forces with their corresponding sloshing height for the roofless tanks shows that the sloshing height calculated for the roofless tanks is less than the freeboard considered for the roofed tanks. Therefore, zero sloshing forces present the sufficiency of the freeboard.

All tanks have similar response variations according to the H/L ratio for the insufficient freeboard cases and zero freeboards. In these tanks, the sloshing forces increase by decreasing the H/L ratio.

Figures 9 and 10 show the time history of the sloshing height at the right and left nodes located at the water's free surface for H10L30 and H5L15 tanks, respectively, under 0.3g scaled Kocaeli earthquake. Three different freeboards are assumed in both figures, including sufficient, 0.25m, and 0.5m freeboards. These figures show that the sloshing

height and its oscillation highly depend on the freeboard assumptions. Comparing sufficient freeboard to two non-zero sufficient ones (0.25m and 0.5m), changes in sloshing height variation trends are noticeable after reaching the sloshing height to the insufficient non-zero freeboard. According to the figures, while maintaining the ratio of length to the height of the tank, the maximum sloshing height is almost the same in both tanks, although there are changes in how water fluctuates. In other words, water oscillates more uniformly in a tank that is shorter in length and height.

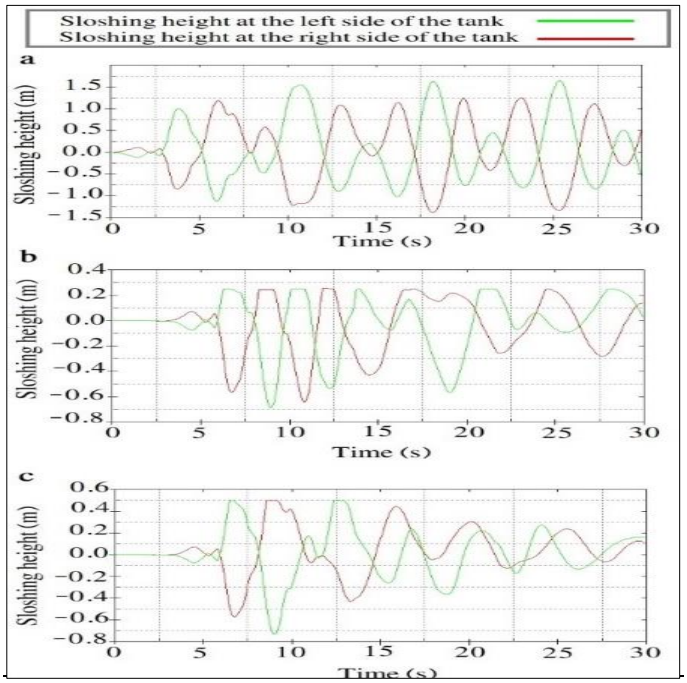

Figure 9. Time history of sloshing height for H10L30 tank under 0.3g scaled Kocaeli earthquake: a) sufficient freeboard, b) 0.25m freeboard, c) 0.5m freeboard

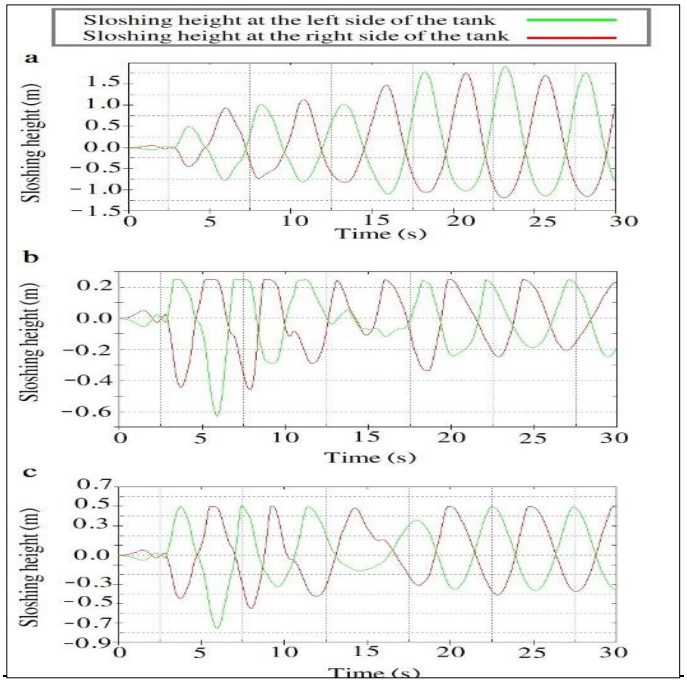

Figure 10. Time history of sloshing height for H5L15 tank under 0.3g scaled Kocaeli earthquake: a) sufficient freeboard, b) 0.25m freeboard, c) 0.5m freeboard

In addition, if the freeboard decreases, the range of water fluctuations becomes more limited, which is expected. It is obvious that when the amplitude of the oscillation equals the amount of freeboard and the sloshing height is positive, the water wave hits the tank's roof.

5.2. The Burial Percentage Effect on the Tank's Response

Burying the tank is another method (other than optimizing the geometric dimensions) used to curb the sloshing

phenomenon and limit the sloshing wave's height. This section studies the impact of the tank's burial percentage on the sloshing height, base shear and moment, and the force applied to the tank's roof.

5.2.1. Sloshing Height Variation

As explained, one impact of the burial condition is the reduction of the heights of the sloshing waves. Under the two different excitations, the model for various burial depths has been analyzed, and the results are presented in Figure 11.

Figure 11 illustrates the variation in sloshing height under different depths of embedding. Generally, the sloshing heights in the tanks on the ground are higher than those perfectly buried, which could be related to the soil's interaction with the container walls. Moreover, as seen in Figure 11, assuming a flexible foundation instead of rigid without burial conditions, the sloshing height increases significantly, proving the foundation rigidity's effects on the sloshing height. It is observed that the embedment of the container and the soil-structure interaction affects the sloshing phenomena. In this study, the soil is assumed to be soft. According to Figure 11, for the embedded depth of more than 50% to 60%, the positive effects of the depth of embedding are more limited; that is, the embedment of more than 60% has no substantial impact on the sloshing height reduction for both earthquake records.

Regarding the differences between the results under the two earthquake records, it should be noted that, unlike the high-frequency earthquake record of Northridge, the lower-frequency earthquake record of Kocaeli affects more the whole convective part of the tank's water, and consequently, sloshing caused by the Kocaeli earthquake record is much higher than the Northridge's since this record is close to the fundamental frequency of the convective part of the liquid in the tanks may result in the resonance phenomenon. Moreover, the first mode natural period of all tank systems, based on the two approaches, is calculated using the FEM software. Also, the convection and impulsive parts periods are obtained using ACI350 codes (Table 3).

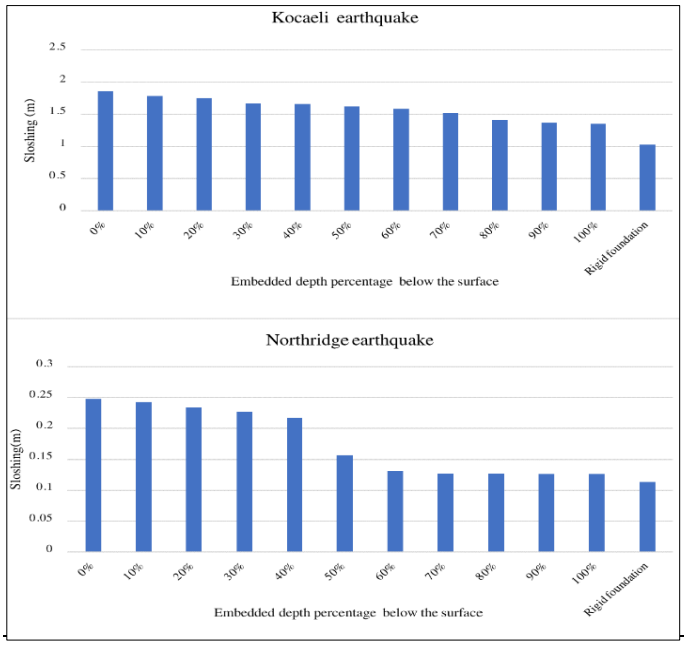

Figure 11. Values of sloshing height changes in the tanker with the effect of changes in the percentage of the burial of the tanks and the rock around the tank wall in the Kocaeli and Northridge earthquake

Table 3. The period of the whole tank system in two approaches, and the convection and impulsive part period are obtained by ACI350 codes

	Convection part (ACI)	Impulsive part (ACI)	Water tank (FEM)
Period (s)	4.8	0.153	0.086

5.2.2. The Forces Applied to the Roof of the Tank

This section includes the forces applied to the roof, and the results obtained are scrutinized to see the effect of the burial approach. For the different burial depths, under the Kocaeli earthquake and in the S3 soil (see Table 2), the maximum forces exerted on the roof have been computed, which are presented in Figure 12. As seen, the force on the roof at zero buried depth is the highest and decreases slightly as the buried depth increases. Of course, it is worth noting that the force is almost constant from a buried depth of 5.6m. Regarding the effect of the freeboard, it can be said that the less freeboard there is, the greater the amount of force on the roof. For the case in which the freeboard is 1m, the amount of force on the roof is approximately 5% of the force in the case in which the freeboard is zero.

Another noteworthy point is that according to Figure 12, in the case where the freeboard is 1m, increasing the buried depth does not significantly change the amount of force exerted on the roof, and it seems that the optimal amount of force occurs in this case. According to the given explanations, the more the freeboard, the less force is applied to the roof, and the less buried depth is required.

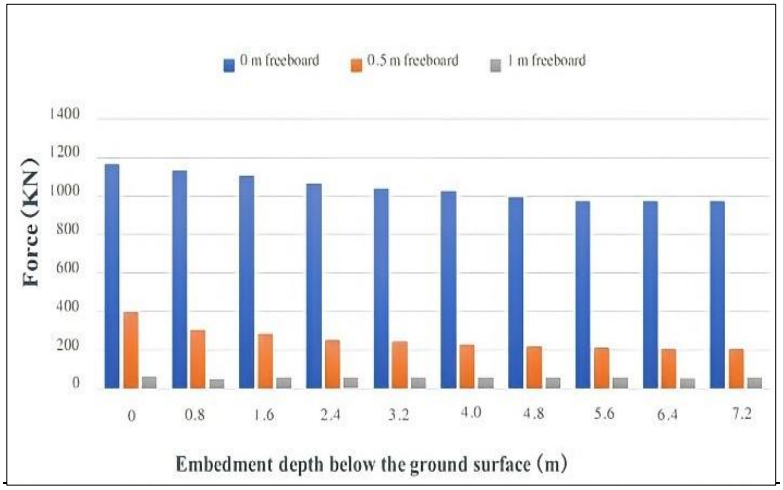

Figure 12. The maximum force applied to the roof of the tank under the Kocaeli earthquake for S3 soil type and different burial depths

5.3. The Baffle Implementation Effect on the Tank

As mentioned earlier, the baffles are implemented to reduce the sloshing-related damage to the tank's structure. In order to examine their effects, the FEM analysis under Kocaeli earthquake records has been conducted, and the results include sloshing wave heights and roof forces which are presented.

5.3.1. The Baffle Effect on the Sloshing Heights

Following the FEM analysis of the tanks and comparing Figure 13 with Figure 7, the displacements of left and right nodes in the free surface of the water demonstrate that the use of baffles has led to a very significant reduction in sloshing height while the tank is located on the surface. This phenomenon can be due to the fact that the tank is divided into several parts by the baffles, which leads to more damping or containment of the water and eventually reduces the height of the sloshing waves.

According to Figure 13, the left node in green experiences more displacement. Since the maximum displacement is small, it is not of paramount importance from a structural engineering point of view. In addition, Figure 14 shows the tank's free surface changes under the earthquake at different times. As shown in the figures and previously explained, the water level changes are minor, demonstrating the efficiency of baffles during earthquakes in controlling sloshing wave height compared to the burial approach. Figure 15 shows the amount of force applied to the baffles. In the left baffle, Figure 15-a, the amount of force is about 36.8kN. Also, in the middle-left baffle, Figure 15-b, this amount reaches 42.6kN. The reason for this difference could be the amount of contained liquid on both sides of the baffles and the presence of the tank wall, which has more stiffness and makes the left baffle absorb less force than the middle-left baffle. In the right and middle right baffles, Figures 15-c and 15-d, the force amount of force equals 37.9kN and 42.8kN, respectively. The difference in the amount of force on these two baffles could be similar to the reason mentioned for the two left baffles.

5.4. The Energy Dissipation of Sloshing Waves

To investigate the energy dissipation of sloshing waves caused by the installation of baffles and changing the geometry under the Kocaeli earthquake, four cases are considered:

1-Installation of the baffles without burial condition (Baffled Tanks)

2-Without baffles in all burial percentage

3-Rigid foundation and without baffles

4-Six unbaffled tanks with different geometry (Figure 7-a))

The energy of the sloshing waves in the unbaffled and baffled cases are indicated by E_S and E_B, respectively [25]. Note that the energy induced by the sloshing waves is directly proportional to the square of the maximum sloshing wave height, η_{max}^2. Therefore, if the maximum sloshing wave heights are shown by $\eta_{max\,S}$ and $\eta_{max\,B}$ for the unbaffled and baffled cases, respectively, the energy dissipation ratio, which is denoted by ξ , is calculated as follows:

$$\xi = [(E_S - E_B)/E_S] \times 100\% = [(\eta_{max\,S}^2 - \eta_{max\,B}^2)/\eta_{max\,S}^2] \times 100\% \quad (15)$$

According to Figures 12 and 14, the unburied condition $\eta_{max\,S}$ is equal to 1.85 m and $\eta_{max\,B}$, which denotes the maximum sloshing wave height for the baffled case, is equal to 0.35 m. By placing the values in Equation 15 we have:

$$\xi = (1.85^2 - 0.35^2)/1.85^2] \times 100\% = 96.42\% \quad (16)$$

Therefore, based on the calculations, implementing the baffles has resulted in the loss of about 96% of the energy of the sloshing waves, which clearly demonstrates the baffles' efficiency. The following results are obtained by doing the same calculations for the different buried depths.As can be seen in Figure 16, even if the burial percentage is 100%, the energy dissipation ratio is still less

than 50%, and if the foundation is assumed to be rigid, it is almost 70%. Therefore, it is evident that using the baffles with an energy dissipation ratio of about 96% shows much better performance.

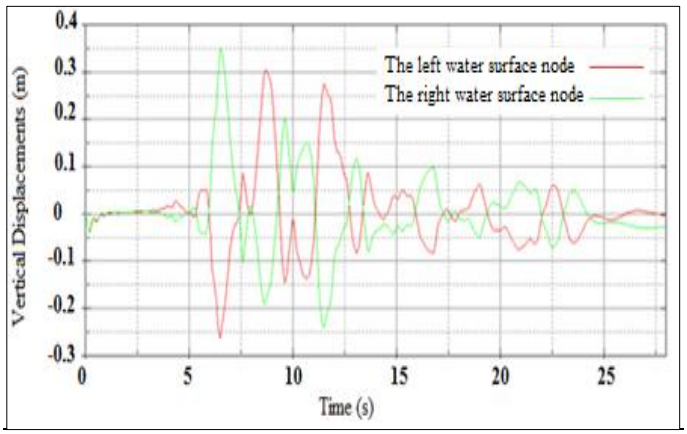

Figure 13. The vertical displacements of the left (red) and right (green) water surface nodes during the Kocaeli earthquake under no burial condition.

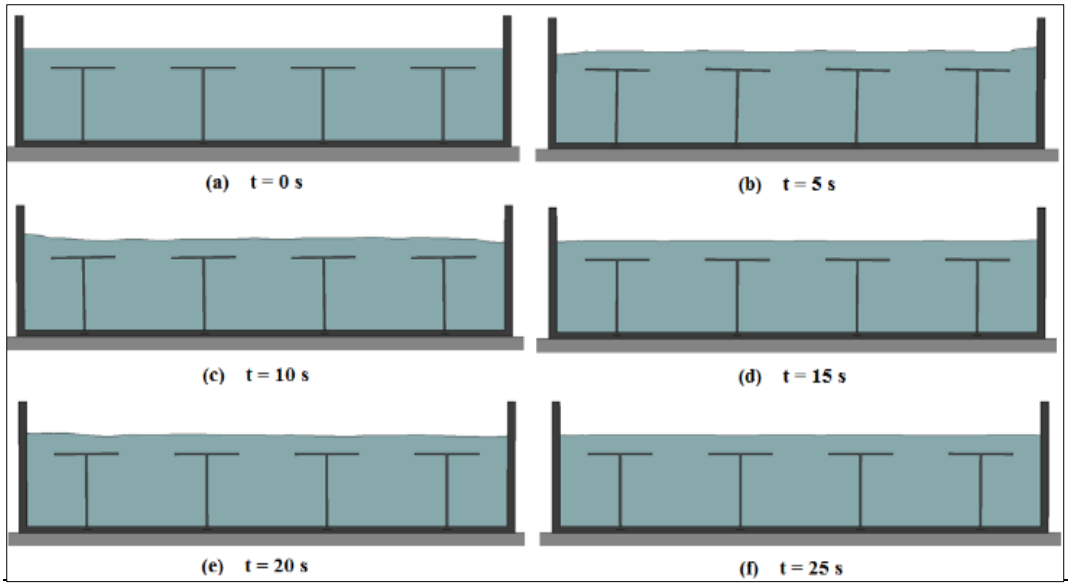

Figure 14. The water surface displacements at different times under the Kocaeli earthquake

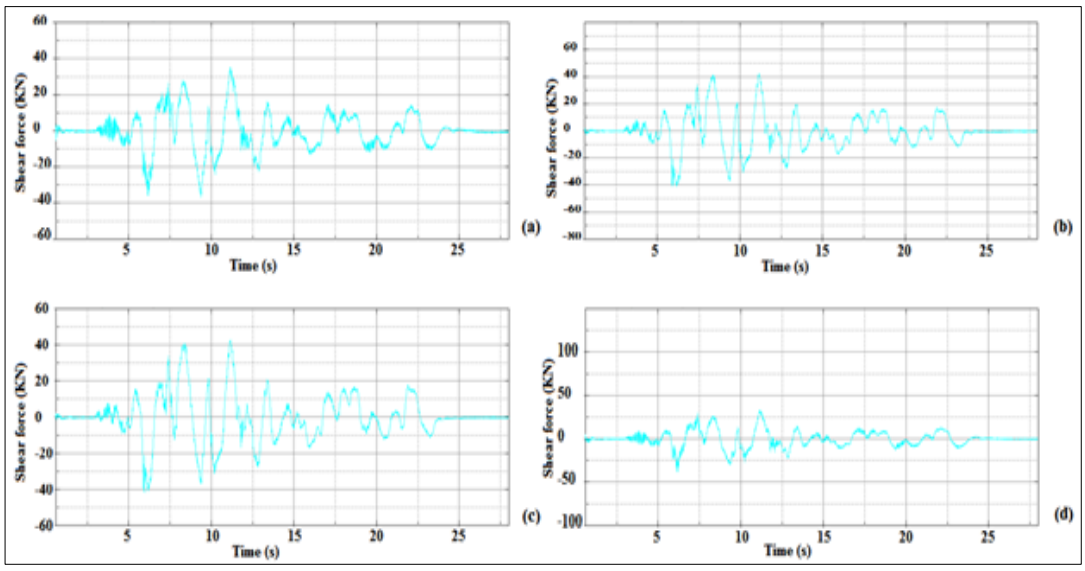

Figure 15. The forces applied to the installed baffles under the Kocaeli earthquake. (a) Water to left baffle force, (b) Water to mid-left baffle force, (c) Water to mid-right baffle force, (d) Water to right baffle force

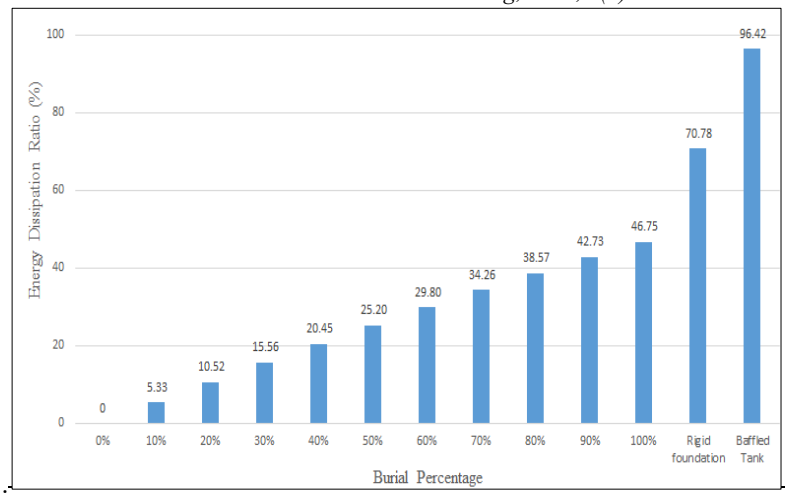

Figure 16. The Energy Dissipation Ratio for different cases of the tank

Finally, in Figure 17, according to Equation 15, the energy dissipation ratios of six different unbaffled tanks have been computed with respect to the H5-L10 tank, which represented the greatest sloshing height, as shown in Figure 7-a. Therefore, the dissipation ratio for the H5-L10 is considered zero. As seen in Figure 17, for the tanks with the same height, the dissipation energy ratio rises significantly as the length of the tank increases. Comparing H5- L30 with H10-L30, it can be said that for the same length, the dissipation energy ratio increases as the height decreases. Moreover, it is observed that for the same length-to-height ratio, the larger the tank, the greater the energy dissipation ratio.

6. Conclusions

This study investigates the factors affecting sloshing height, methods to reduce it, and its consequences, including the force on the tank roof. To this end, the geometric properties and methods of the tank's burial and installation of T-shaped baffles were investigated. Finally, using the concept of dissipated energy ratio, the efficiency of the two burial methods and the use of T-shaped baffles were compared. Some of the important results of this research are as follows:

1- The maximum sloshing height decreases with increasing the tank length for the constant H. Furthermore, for the fixed L, the maximum sloshing height increases with increasing the tank height. Hence, decreasing the H-to-L ratio of the tank leads to reducing the maximum sloshing height.

2- Compared with the Northridge, the Kocaeli earthquake component causes higher response spectrum acceleration over the first convective mode of sloshing, meaning that the seismic excitation's frequency content significantly affects the sloshing phenomena.

3- Comparing the dimensions of the tanks, the larger the tank, the greater the fundamental period.

4- For the embedded depth of more than 50% to 60%, the positive effects of the depth of embedding are more limited; that is, the embedment of more than 60% has no substantial impact on the sloshing height reduction for both earthquake records.

5- In comparison to the burial approach, the use of baffles has led to a very significant reduction in sloshing height while the tank is located on the surface. According to the definition of energy dissipation ratio, even if the burial percentage is 100%, the energy dissipation ratio is still less than 50%. Assuming the foundation to be rigid, the energy dissipation ratio is nearly 70%. Therefore, it is evident that utilizing the baffles with an energy dissipation ratio of about 96% provides much better efficiency.

6- Considering the geometric effects on sloshing height, it is seen that for the same length-to-height ratio, the larger the tank, the greater the energy dissipation ratio.

As mentioned before, the aim of this study is to provide a more comprehensive insight into different approaches typically used to limit the damages due to the sloshing phenomenon. However, it is blatantly obvious that owing to the complex nature of engineering structures such as tanks, the ultimate choice is left to the engineers' judgment.

7. References

[1] Li, Y. C., & Gou, H. L. (2018). Modeling Problem of Equivalent Mechanical Models of a Sloshing Fluid. Shock and Vibration, *2018*. doi:10.1155/2018/2350716.

[2] Altunisik, A. C., & Sesli, H. (2015). Dynamic response of concrete gravity dams using different water modelling approaches: Westergaard, lagrange and euler. Computers and Concrete, *16*(3), 429–448. doi:10.12989/cac.2015.16.3.429.

[3] Moslemi, M., Farzin, A., & Kianoush, M. R. (2019). Nonlinear sloshing response of liquid-filled rectangular concrete tanks under seismic excitation. Engineering Structures, *188*, 564–577. doi:10.1016/j.engstruct.2019.03.037.

[4] Mas'ud Alfanda, A. (2017). Comparative Analysis of Circular and Rectangular Reinforced Concrete Tanks Based on Economical Design Perspective. American

Journal of Applied Scientific Research, *3*(2), 14. doi:10.11648/j.ajasr.20170302.12.

[5] Kim, J. K., Koh, H. M., & Kwahk, I. J. (1996). Dynamic Response of Rectangular Flexible Fluid Containers. Journal of Engineering Mechanics, *122*(9), 807–817. doi:10.1061/(asce)0733-9399(1996)122:9(807).

[6] Chern, M. J., Vaziri, N., Syamsuri, S., & Borthwick, A. G. L. (2012). Pseudospectral solution of three-dimensional nonlinear sloshing in a shallow water rectangular tank. Journal of Fluids and Structures, *35*, 160–184. doi:10.1016/j.jfluidstructs.2012.08.003.

[7] Camnasio, E., Orsi, E., & Schleiss, A. J. (2011). Experimental study of velocity fields in rectangular shallow reservoirs. Journal of Hydraulic Research, 49(3), 352–358. doi:10.1080/00221686.2011.574387.

[8] Ghateh, R., Kianoush, M. R., & Pogorzelski, W. (2015). Seismic response factors of reinforced concrete pedestal in elevated water tanks. Engineering Structures, *87*, 32–46. doi:10.1016/j.engstruct.2015.01.017.

[9] Hadj-Djelloul, N., & Djermane, M. (2020). Effect of geometric imperfection on the dynamic of elevated water tanks. Civil Engineering Journal (Iran), *6*(1), 85–97. doi:10.28991/cej-2020-03091455.

[10] Wang, Q., Tiwari, N. D., Qiao, H., & Wang, Q. (2020). Inerter-based tuned liquid column damper for seismic vibration control of a single-degree-of-freedom structure. International Journal of Mechanical Sciences, *184*, 105840. doi:10.1016/j.ijmecsci.2020.105840.

[11] Dou, P., Xue, M. A., Zheng, J., Zhang, C., & Qian, L. (2020). Numerical and experimental study of tuned liquid damper effects on suppressing nonlinear vibration of elastic supporting structural platform. Nonlinear Dynamics, *99*(4), 2675–2691. doi:10.1007/s11071-019-05447-y.

[12] Jin, X., Tang, J., Tang, X., Mi, S., Wu, J., Liu, M., & Huang, Z. (2020). Effect of viscosity on sloshing in a rectangular tank with intermediate liquid depth. Experimental Thermal and Fluid Science, *118*, 110148. doi:10.1016/j.expthermflusci.2020.110148.

[13] Shekari, M. R. (2020). On the numerical assessment of the resonant sloshing responses in 3D multi baffled partially liquid-filled steel cylindrical tanks shaken by long-period ground motions. Soil Dynamics and Earthquake Engineering, *129*, 105712. doi:10.1016/j.soildyn.2019.105712.

[14] Yu, L., Xue, M. A., & Jiang, Z. (2020). Experimental investigation of parametric sloshing in a tank with vertical baffles. Ocean Engineering, *213*, 107783. doi:10.1016/j.oceaneng.2020.107783.

[15] Ünal, U. O., Bilici, G., & Akyıldız, H. (2019). Liquid sloshing in a two-dimensional rectangular tank: A numerical investigation with a T-shaped baffle. Ocean Engineering, *187*, 106183. doi:10.1016/j.oceaneng.2019.106183.

[16] Aghajanzadeh, S. M., Mirzabozorg, H., & Yazdani, H. (2023). SPH Technique to Study the Sloshing in Concrete Liquid Tanks. Numerical Methods in Civil Engineering, *8*(1), 1–17. doi:10.61186/nmce.2304.1015.

[17] Wang, G., Lu, W., Zhang, S. (2021). Seismic Potential Failure Mode Analysis of Concrete Gravity Dam–Water–Foundation Systems Through Incremental Dynamic Analysis. In: Seismic Performance Analysis of Concrete Gravity Dams. Advanced Topics in Science and Technology in China,. Springer, Singapore. doi:10.1007/978-981-15-6194-8_4.

[18] Kianoush, M. R., & Ghaemmaghami, A. R. (2011). The effect of earthquake frequency content on the seismic behavior of concrete rectangular liquid tanks using the finite element method incorporating soil-structure interaction. Engineering Structures, *33*(7), 2186–2200. doi:10.1016/j.engstruct.2011.03.009.

[19] Jia, J. (2016). Modern earthquake engineering: Offshore and land-based structures. Springer, Cham, Switzerland.

[20] ACI 350.3-01. (2001). Seismic Design of Liquid-Containing Concrete Structures, Reported by ACI Committee 350, Environmental Engineering Concrete Structures. American Concrete Institute (ACI), Michigan, United States.

[21] Vesenjak, M., Mullerschon, H., Hummel, A., & Ren, Z. (2004). Simulation of fuel sloshing-comparative study. LS-DYNA Anwenderforum, 1-8.

[22] Ghaemmaghami, A. (2010). Dynamic time-history response of concrete rectangular liquid storage tanks. PhD Thesis, Sharif University, Tehran, Iran.

[23] Livaoglu, R., Cakir, T., Dogangun, A., & Aytekin, M. (2011). Effects of backfill on seismic behavior of rectangular tanks. Ocean Engineering, *38*(10), 1161–1173. doi:10.1016/j.oceaneng.2011.05.017.

[24] Elnashai, A. S., & Di Sarno, L. (2008). Fundamentals of Earthquake Engineering. John Wiley & Sons, Hoboken, United States. doi:10.1002/9780470024867

[25] Xue, M.-A., Zheng, J., & Lin, P. (2012). Numerical Simulation of Sloshing Phenomena in Cubic Tank with Multiple Baffles. Journal of Applied Mathematics, 2012(1). doi:10.1155/2012/245702.